HIGH-TEMPERATURE STRAIN GAUGE MEASUREMENTS IN WA-DED: VALIDATION OF NUMERICAL MODELS

H. DREXLER*, M. MOSCHINGER**, N. ENZINGER**

** LKR Leichtmetall Kompetenzzentrum Ranshofen GmbH, 5282 Braunau am Inn - Ranshofen, Austria*
*** Institute of Materials Science, Joining and Forming, Graz University of Technology, 8010 Graz, Austria*

DOI 10.3217/978-3-99161-089-2-023, license CC BY 4.0
https://creativecommons.org/licenses/by/4.0/deed.en
This CC license does not apply to third party material and content noted otherwise.

ABSTRACT

In this study, high-temperature strain gauges are used to monitor the in-situ stress during plasma Wire Arc Directed Energy Deposition (WA-DED). A computational temperature compensation is applied to correct the strain signals for thermal effects, enabling accurate stress measurements at high temperatures. The experimental results are compared against a fully coupled thermo-mechanical finite element simulation.

The comparison shows good agreement between measured and simulated stresses, demonstrating that high-temperature strain gauges can reliably capture the stress evolution during WA-DED. This approach goes beyond conventional post-process residual stress measurements by providing time-resolved validation data. The findings underline the potential of in-situ high-temperature strain gauge measurements as a robust tool for validating WA-DED simulations.

Keywords: WA-DED, numerical simulation, strain gauge, in-situ stress measurements

INTRODUCTION

Wire Arc Directed Energy Deposition (WA-DED) is an additive manufacturing technology that enables the production of large, complex shaped metallic components [1]. The process is characterized by a localized heat input from the arc and the subsequent solidification shrinkage of the deposited material. Both effects lead to the development of residual stresses and distortions, which can significantly influence the mechanical performance and dimensional accuracy of the final component [2]. Understanding and controlling these thermo-mechanical phenomena is therefore crucial to ensure component reliability and to enable the wider industrial adoption of WA-DED.

Numerical simulations have become an important tool for predicting temperature fields, stress evolution, and distortions in WA-DED. Such models allow virtual process optimization,

reducing the need for extensive experimental trial-and-error studies. A key challenge, however, lies in the reliable validation of these simulations. Conventionally, residual stresses are determined by post-manufacturing measurement techniques such as neutron diffraction, X-ray diffraction, hole-drilling, or sectioning methods [3]. These techniques only capture the final residual stress state and thus offer no insight into the transient stress and deformation evolution during deposition. This limitation restricts the validation of numerical models to the final result, leaving uncertainties about the accuracy of the predicted stress history.

For a more comprehensive validation, in-situ measurements during the process are required. Previous approaches have used in-situ digital image correlation (DIC) during the manufacturing process [4], [5]. While DIC enables full-field strain measurements, it requires a complex experimental setup and unhindered visibility of the surface, which limits its applicability in WA-DED. In this context, high-temperature strain gauges offer a promising solution. A prior study has already demonstrated their potential for capturing stress evolution during welding of a single seam [6].

In this study, high-temperature strain gauges are used to measure transient strain fields in a one-sided clamped S355J2 steel substrate during plasma WA-DED. The experimental setup additionally includes a displacement sensor and thermocouples to capture the thermal and mechanical response of the specimen. The measured data are compared with a fully coupled thermo-mechanical finite element simulation performed in Simufact Welding®.

The results demonstrate the feasibility and importance of using high-temperature strain gauges for in-situ validation of WA-DED simulations, contributing to improved predictive modeling in additive manufacturing

WA-DED EXPERIMENT

A series of three trials was conducted in which a four-layer wall was deposited on a one-sided clamped substrate using the plasma WA-DED process (Fig. 1). The substrates were made of S355J2 structural steel with dimensions of 290 mm × 65 mm × 15m. Prior to welding, all substrates were stress-relief heat treated for two hours at 570 °C to eliminate residual stresses. After heat treatment, the substrates were sandblasted and cleaned. The specimens were clamped between a steel base block and a clamping jaw. The block was machined with a positioning step to ensure reproducible alignment of the substrates. The wire material was ER70S-6 (EMK6, voestalpine Böhler Welding GmbH) with a diameter of 1 mm, selected due to its comparable mechanical properties to the substrate. All deposition experiments were carried out on the SBI M3DP-SL machine at TU Graz. The welding parameters were kept constant across all trials, with a wire feed speed of 50 mm/s, a travel speed of 5 mm/s, a current of 260 A, and a voltage of 25 V. To allow for partial cooling before deposition continued, an interlayer dwell time of 828 s was applied between subsequent layers. The final deposit had dimensions of approximately 250 mm × 8 mm × 6 mm (four single track layers).

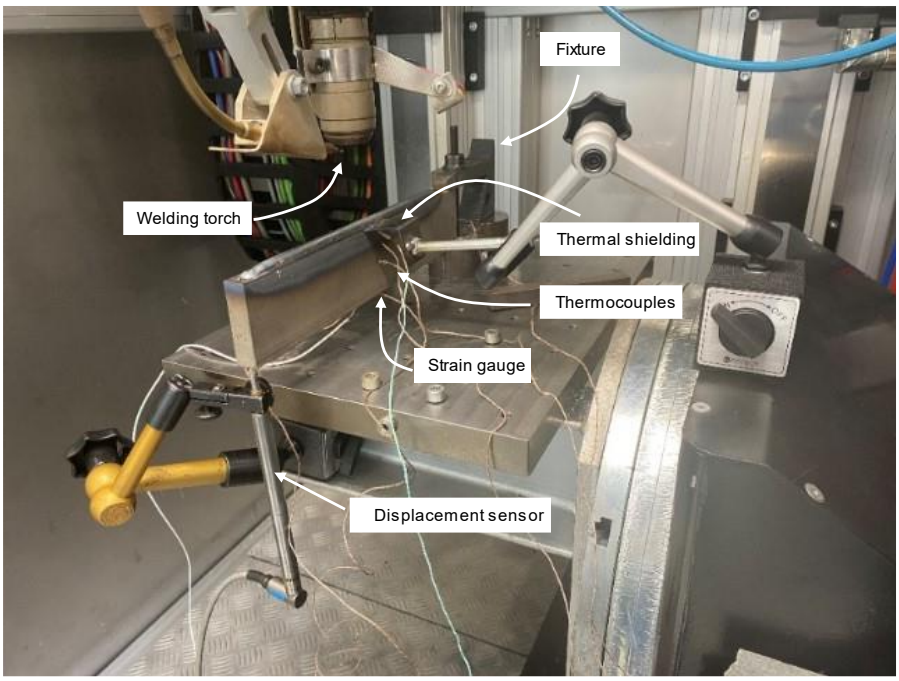

Fig. 1 Experimental setup

TEMPERATURE MEASUREMENTS

The thermal history was recorded using spot-welded Type K thermocouples. Five thermocouples were attached directly to the substrate at the positions shown in Fig. 2.

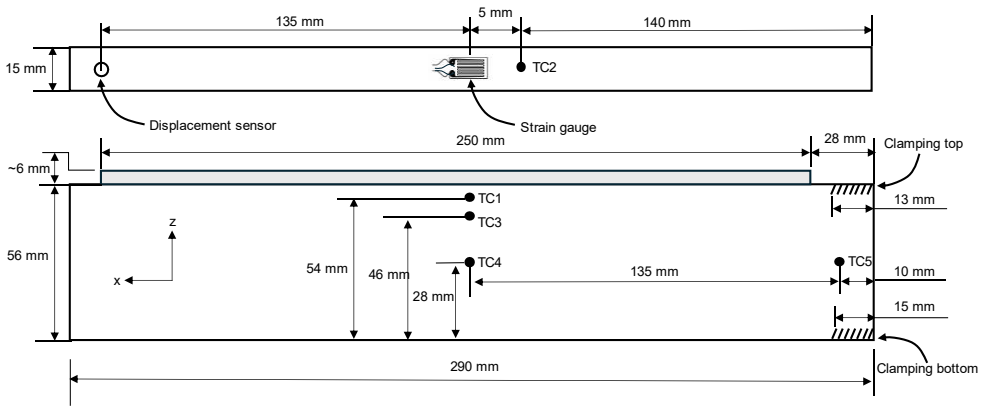

Fig. 2 Substrate dimensions and location of thermocouples, displacement sensor and strain gauge

To protect the thermocouples from direct exposure to the plasma gas, a small metal shield was installed. In addition, two further thermocouples were mounted on the clamping block and the top clamp to monitor the heat flux into the fixtures. Thermal data acquisition was performed partly using an HBM QuantumX MX440B unit and partly with the integrated data acquisition system of the SBI M3DP-SL machine, both operated at a sampling frequency of 5 Hz.

DISPLACEMENT MEASUREMENTS

Vertical displacements of the substrate were measured with an HBM WA20 displacement sensor, which was positioned at the bottom of the free end of the substrate (Fig. 2). The sensor signals were recorded with an HBM QuantumX MX440B unit at a sampling frequency of 5 Hz.

STRESS MEASUREMENTS

Stresses were measured using linear high-temperature foil gauges, combined with computational compensation of the measurement signal, as described later. The gauges were mounted at the center of the bottom surface of the substrate in longitudinal orientation (see Fig. 2 and Fig. 3). Linear gauges were chosen because, at the measurement position, the strain state can be approximated as one-dimensional and thermoelastic in the longitudinal direction. This approximation is justified by the cantilever-like geometry of the substrate, the longitudinal deposition path, and the large distance to the weld bead. All gauges were taken from the same production batch to minimize variability. The main specifications are summarized in Table 1.

Fig. 3 Mechanical clamping for curing under pressure (left), installed gauge and thermocouple (right)

Table 1 Main specifications strain gauges

Parameter	Specification
Type	HBM 1-LM11-6/350GE
Nominal resistance R_0	350 Ω ± 0.3 %
K-factor k	2.38 ± 1 %
Temperature coefficient of K-factor α_k	-406 ± 10 [10^{-6} K^{-1}]
Thermal expansion coefficient of the gauge α_{gauge}	α ≈ 10.8 [10^{-6} K^{-1}]
Combined standard uncertainty u_c	0.6 · ΔT
Polynomial coefficients for intrinsic thermal output $\varepsilon_s(T)$	a_0 = -44.12, a_1 = 2.89, a_2 = -0.0357, a_3 = 5.85×10^{-5}, a_4 = -5.16×10^{-9}
Gauge factor used for polynomial k_{poly}	2
Reference temperature T_{ref}	20 °C
Maximum operating temperature	250 °C (zero-point-related) 300 °C (non-zero-point-related, < 5 h)

Prior to bonding, the substrate surfaces were sanded and cleaned to ensure proper adhesion. The gauges were bonded using a two-component epoxy adhesive (HBM EP310N). The curing procedure was carried out in two stages: first, under pressure with mechanical clamping at 180 °C for two hours, and subsequently a precision curing cycle at 280 °C for two hours without pressure, followed by slow cooling inside the furnace. Pre-trials demonstrated that this precision curing procedure was essential to ensure reliable high-temperature measurements.

Thermocouple TC2 was placed directly next to the gauges to record the local temperature, which was required for the computational temperature compensation. Signal acquisition was performed using an HBM QuantumX MX1615B unit in a 4-wire configuration. The 4-wire configuration compensates for resistance changes in the lead wires that may occur due to thermal influences or differences in cable length. The data was recorded at a sampling frequency of 5 Hz.

MICROGRAPHS

After the welding experiments, cross-sectional micrographs of the weld beads were prepared to characterize the fusion zone and the heat-affected zone. This microstructural information was subsequently used for calibration of the simulation.

TEMPERATURE COMPENSATION

Accurate stress measurements at elevated temperatures require compensating for the thermal effects inherent to strain gauges. Without such corrections, the recorded strain signal may no longer represent the true mechanical response but instead include temperature-induced measurement errors. To ensure reliable results in the WA-DED experiments, a computational temperature compensation was applied.

In absence of temperature effects, strain gauges measure strain ε via the relationship [7]

$$\varepsilon = \frac{\Delta R/R_0}{k} \tag{1}$$

where ΔR denotes the resistance change, R_0 the nominal resistance of the gauge, and k the nominal gauge factor. Assuming purely elastic, uniaxial loading, the corresponding stress σ can then be calculated via Hooke's law as

$$\sigma = E * \varepsilon \tag{2}$$

with E being the Young's modulus of the substrate material.

However, during temperature changes, strain gauges measure an apparent strain, even when no mechanical load is present. The apparent strain originates from three main sources:

1. The temperature dependence of the gauge's K-factor
2. Mismatches in the coefficients of thermal expansion (CTE) between the substrate and the gauge, and
3. The intrinsic thermal output of the gauge itself.

To account for the apparent strain at higher temperatures, it is necessary to measure the temperature at the strain gauge location an apply an additional computational correction to the signal [8].

The temperature dependent K-factor $k^*(T)$ is described as

$$k^*(T) = k \cdot \left(1 + \alpha_k (T - T_{\mathrm{Ref}})\right) \tag{3}$$

where $k^*(T)$ is the effective K-factor at temperature T, α_k is the temperature coefficient of the gauge factor, and T_{Ref} is the reference temperature.

Strain resulting from the thermal expansion mismatch is given by

$$\varepsilon_f(T) = \left(\alpha_{\mathrm{substrate}} - \alpha_{\mathrm{gauge}}\right) \cdot \Delta T \tag{4}$$

where $\alpha_{\mathrm{substrate}}$ and α_{gauge} are the thermal expansion coefficients of the substrate and the strain gauge, respectively.

The intrinsic thermal output of the gauge is usually given by the manufacturer as a polynomial function of temperature:

$$\varepsilon_s(T) = (\mathrm{a}_0 + \mathrm{a}_1\mathrm{T} + \mathrm{a}_2\mathrm{T}^2 + \mathrm{a}_3\mathrm{T}^3 + \ldots) \cdot \frac{k_{\mathrm{poly}}}{k^*(T)} \tag{5}$$

with coefficients a_n provided in the datasheet. Since this polynomial is defined for a fixed reference K-factor k_{poly}, it must be rescaled to the actual temperature-dependent K-factor by multiplying with the ratio $\frac{k_{\text{poly}}}{k^*(t)}$.

Combining these contributions, the corrected strain signal is obtained as

$$\varepsilon_c(T) = \varepsilon \frac{k}{k^*(T)} - \varepsilon_f(T) - \varepsilon_s(T) \tag{6}$$

Finally, in converting compensated strain to stress, the temperature dependence of the Young's modulus $E(T)$ must also be considered:

$$\sigma_C = E(T) \cdot \varepsilon_c(T) \tag{7}$$

FURNACE EXPERIMENT

To validate the computational temperature compensation and to quantify the influence of thermal effects, a dedicated furnace experiment was conducted prior to the WA-DED deposition trials. In addition, this test was used to determine the coefficient of thermal expansion of the substrate material.

For this purpose, the three substrates equipped with strain gauges and thermocouples were placed inside a chamber furnace (Fig. 4). The specimens were heated to a maximum temperature of 250 °C at a controlled heating rate of 2 °C/min, ensuring a slow and uniform temperature increase. The heating rate was kept low to ensure that thermal equilibrium was maintained throughout the samples, thereby avoiding the generation of additional thermal stresses.

During the entire heating cycle, strain and temperature were recorded simultaneously at the strain gauge location, allowing the characterization of apparent strain in the absence of mechanical loading.

Fig. 4 Substrates with installed strain gauges in chamber furnace

Fig. 5 shows the mean measured strain ε_{mean} together with the standard deviation σ_{std} of the three gauges without any compensation. For comparison, the combined standard uncertainty u_c specified in the datasheet is also applied to the mean curve and displayed. The experimental standard deviation remains well within the datasheet uncertainty band, confirming the repeatability of the measurements.

Since the selected strain gauge was designed to have a coefficient of thermal expansion closely matching that of the substrate material, the measured strain remains close to zero near room temperature, as expected. However, with increasing temperature, a negative apparent strain develops. This behavior can be attributed to small mismatches in the coefficients of thermal expansion, the temperature dependence of the gauge's K-factor, and the intrinsic thermal output of the strain gauge.

The results highlight that temperature compensation becomes increasingly important at elevated temperatures. At 200 °C, the apparent thermal strain reaches approximately 230 µm/m, which corresponds to about 48.3 MPa when assuming a Young's modulus of 210 GPa. In theory, the datasheet's combined standard uncertainty could add an additional error of roughly ±25 MPa.

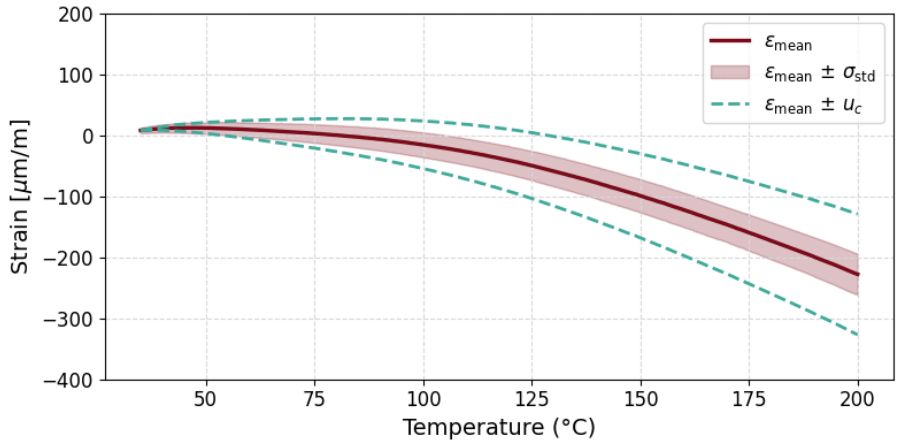

Fig. 5 Furnace experiment - uncompensated strain

Fig. 6 shows the compensated mean strain $\varepsilon_{c,mean}$ curve according to Eqn. (6) along with the individual correction components. Among these, the polynomial correction ε_s, which compensates for the intrinsic thermal output of the strain gauge, has the largest influence, followed by the correction for the coefficient of thermal expansion ε_f. The temperature dependence of the K-factor, on the other hand, contributes only marginally and could therefore be neglected.

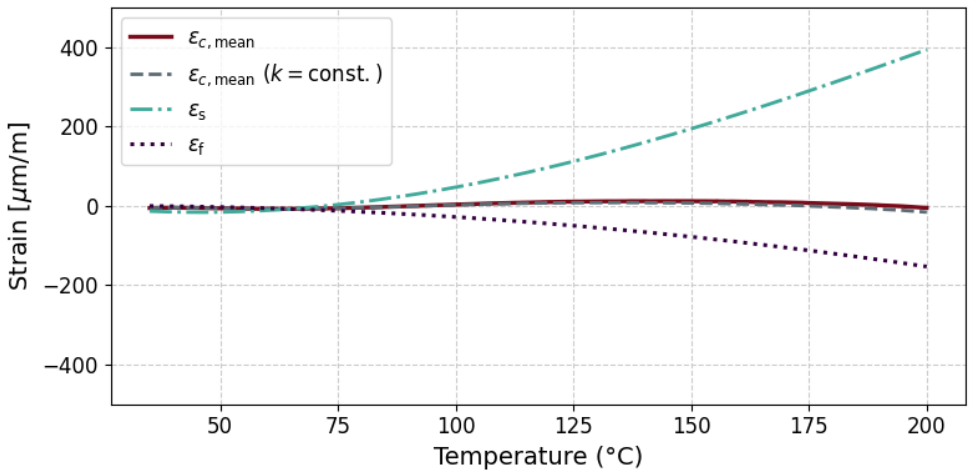

Fig. 6 Furnace experiment - compensated strain and individual correction contributions

For the temperature compensation, the linear coefficient of thermal expansion of the substrate material $\alpha_{substrate}$ was treated as an unknown parameter. It was fitted such that the

compensated mean strain $\varepsilon_{c,mean}$ is minimized. Fig. 7 compares the fitted linear coefficient of thermal expansion with literature data for a similar material.

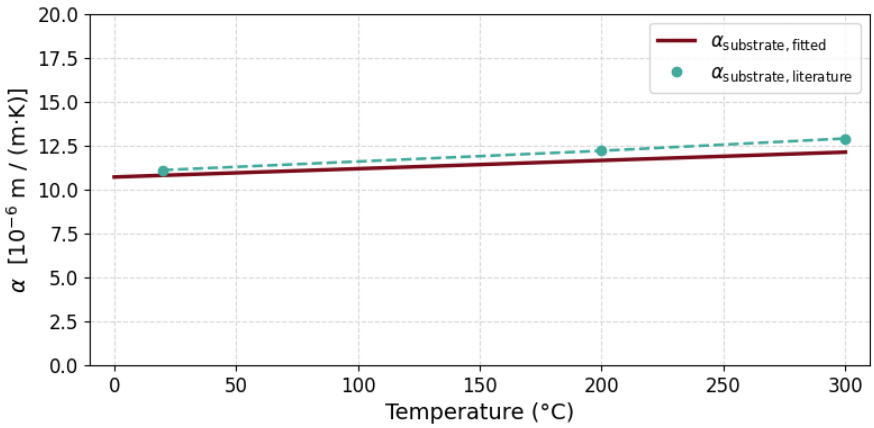

Fig. 7 Coefficient of thermal expansion of the substrate - fitted from furnace experiment compared to literature data [9]

The results show good agreement. This indicates that the compensation equations were implemented correctly. Possible reasons for the slight underestimation are small differences in the material composition, uncertainties of the strain gauges, or the ambient conditions at the start of the experiment. The strain measurements were zeroed at an environmental temperature of 30 °C, while both the literature values and the datasheet polynomial are referenced to 20 °C.

NUMERICAL MODEL

A fully coupled thermo-mechanical finite element (FE) analysis of the additive manufacturing process was performed using the commercial software Simufact Welding®.

The finite element model is shown in Fig. 8. In addition to the substrate and deposited welds, the fixture and welding table were also included. To reduce complexity, the weld seams were modeled as rectangular layers with a width of 8 mm and a height of 1.4 mm. The mesh size was set to 2 mm in the substrate and 1 mm in the weld seam. An automatic refinement algorithm was applied to locally refine the mesh in regions with steep thermal gradients. The time step size was adaptive, with a maximum step size limited to 0.5 s.

BOUNDARY CONDITIONS

No clamping force is considered in this model. Instead, movement of the nodes along the contact area of the fixture is prohibited using single point constraints. Hence, the fixture acts solely as a thermal heat sink. The heat transfer coefficient between bodies in contact was set to 5000 W/m²K.

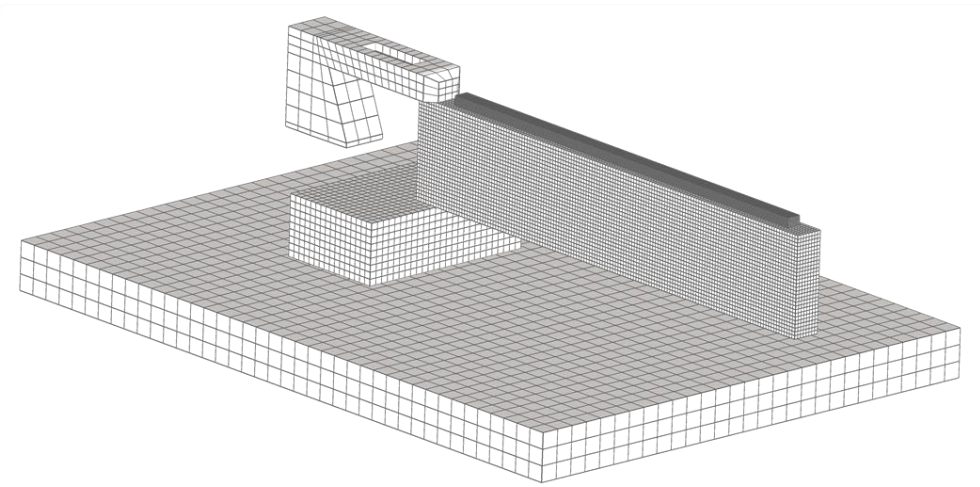

Fig. 8 Finite element model

Convective and radiative boundary conditions are applied to all outer surfaces. The materials emissivity and the convection coefficient are assumed independent of the temperature and set to 0.7 and 6.5 W/m²K, respectively. The heat transfer coefficients and thermal boundary conditions were calibrated by trial and error, until the temperatures in the simulation are in good agreement with the temperatures measured in the experiments.

HEAT SOURCE MODELLING

In this study the energy input during the WA-DED process was represented by a moving cylindrical heat source. This model is a simplification of the three-dimensional conical heat source model (TDC) [10]. It defines the volumetric heat generation rate Q_V by a Gaussian distribution as

$$Q_V(r) = Q_0 \cdot \exp\left(-\frac{Mr^2}{r_0^2}\right) \tag{8}$$

where M is the Gaussian parameter, r_0 the radius of the cylinder and r the radial coordinate. The maximum heat intensity Q_0 is given by

$$Q_0 = \frac{3\eta P e^3}{dr^2\pi(e^3-1)} \tag{9}$$

Here, P denotes the power input, η the process efficiency and d the cylinder height. In cases where parts of the heat source extended beyond the calculation mesh, the total heat input was scaled to ensure that the net input energy matched the defined process power.

The heat source path was defined using nodes of the calculation mesh. This approach was necessary because of the large displacements occurring in the cantilever experiment, ensuring that the heat source moved consistently with the deforming mesh.

In the present study the process efficiency was set to $\eta = 0.47$ and was calibrated, similar to the other boundary conditions, by comparing simulated and measured temperature curves. The cylindrical heat source was defined with $r_0 = 9\,mm$, $d = 2\,mm$ and a Gaussian parameter of $M = 1$. Fig 9 compares the experimental cross-sectional micrograph with the simulated maximum temperature distribution, showing that the chosen heat source dimensions reproduce the fusion zone with good agreement.

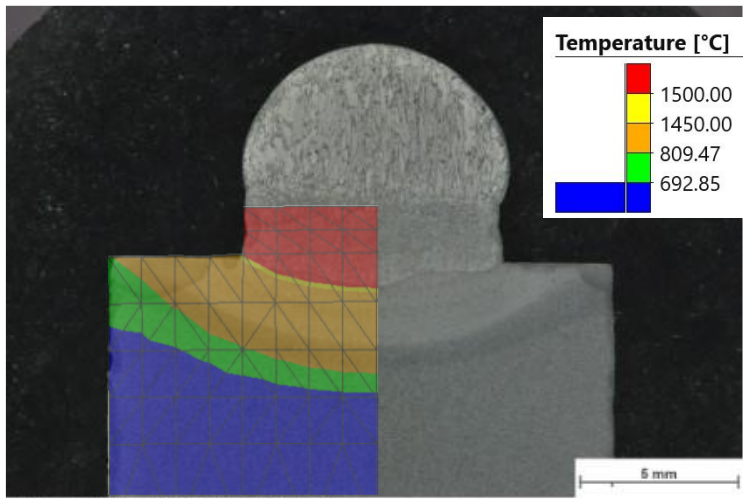

Fig. 9 Cross-sectional micrograph of the deposited wall compared with the maximum temperature distribution from the simulation.

MATERIAL MODELLING

The thermo-mechanical behavior was described using a fully coupled thermo-elasto-plastic constitutive model as implemented in Simufact Welding®. Elastic behavior was modeled as linear isotropic elasticity with temperature-dependent Young's modulus and Poisson's ratio. Plastic deformation was governed by a von Mises yield criterion with isotropic hardening, using temperature-dependent flow curves provided by the Simufact material database. Thermal strains were calculated based on the temperature-dependent coefficient of thermal

expansion. Phase transformations were neglected, and therefore no transformation-induced strains or transformation plasticity effects were considered.

The deposition of material was modeled using the quiet element method [11]. In this approach, all deposit elements are included in the mesh from the beginning but are initially set to a "quiet" state, where they do not significantly affect the analysis (e.g., very low thermal conductivity and Young's modulus). As these quiet elements are heated by the moving heat source, their actual thermo-physical properties are activated, thereby mimicking the material deposition process.

State-of-the-art WA-DED simulations often employ the dead element method. In this approach, deposit elements are initially removed from the calculation and are gradually added (e.g., layer by layer) before being activated in the same way as in the quiet element method. This strategy significantly reduces computational effort in the early stages of the simulation. However, it is not well suited for cases involving large deformations, since nodes of new elements are added with their original coordinates. As a consequence, highly distorted or even negative-volume elements may occur.

RESULTS

This section presents the results of the three WA-DED trials alongside the corresponding FEM simulation. Experimental results are shown as mean values, with the standard deviation reflecting the scatter between the repetitions.

THERMAL HISTORY

Figure 10 shows exemplary results from two thermocouples (TC1 and TC2) for both experiment and simulation. TC1 is closest to the molten pool, TC2 is located at the strain-gauge position. For the far-field location (TC2), the experimental measurements show only minor scatter between the three trials, indicating good repeatability at the strain-gauge position. In contrast, near the molten pool (TC1) the measurements show significant differences (up to ~150 °C) in peak temperature. Possible reasons are direct interaction with the plasma gas and slight positioning differences. Because of the steep thermal gradients near the pool, even small position offsets can lead to substantial temperature differences. At TC1 location, the simulation predicts a maximum temperature gradient of 95 °C/mm, so an offset of less than 1.6 mm could already cause a deviation of 150 °C. The temperature at strain-gauge location remains within the datasheet's maximum allowable temperature of 250 °C.

Overall, the simulated temperature histories agree well with the mean experimental curves, supporting the adequacy of the thermal calibration and the thermophysical properties used in the model. Measurements from the remaining thermocouples also show similarly good agreement with the simulation.

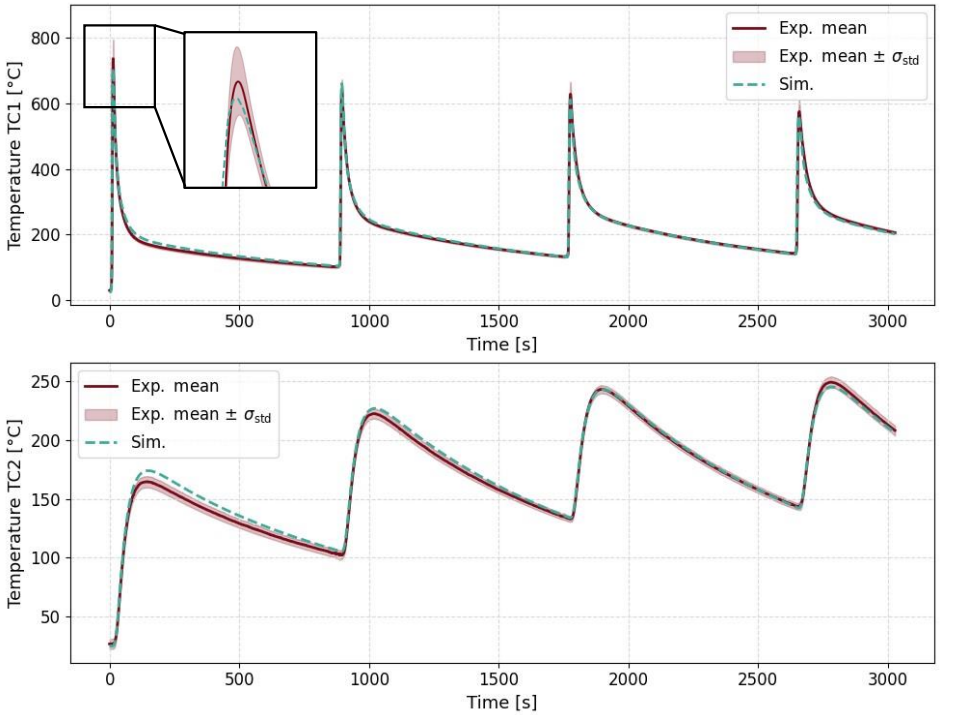

Fig. 10 Thermal history of thermocouples TC1 and TC2 - experiment vs simulation

DISPLACEMENT HISTORY

Fig. 11 compares the experimental and simulated vertical displacements at the contact point of the displacement sensor. The small scatter between trials demonstrates the good reproducibility of the setup. At the beginning of the welding process, the substrate bent downward due to the higher thermal expansion of the top surface relative to the bottom. As deposition continued, the substrate gradually bent upward, primarily driven by solidification shrinkage of the deposited weld seam. This downward–upward sequence repeated with each layer, with most of the displacement occurring after the first layer. This behavior is consistent with observations from a previous study [12]. The simulation captured the overall trend but tended to slightly overpredict the downward bends and underpredict the upward bends. Possible reasons include variations in substrate properties, limitations of the material model that neglected phase transformations, an imperfect heat-source representation, and general modeling simplifications."

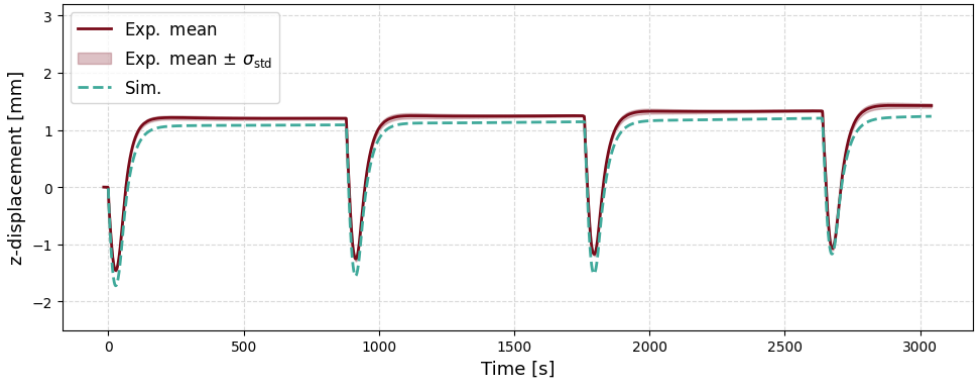

Fig. 11 Displacement history - experiment vs simulation

Stress history

As illustrated in Fig. 12, the stress evolution measured by the strain gauges shows the same qualitative pattern as the displacement history. Scatter between the trials was small, again confirming the reproducibility of the measurements. The largest scatter occurred immediately after each layer was deposited. A possible explanation is that these are the moments of highest temperature, where the deviation of the strain measurement is also most pronounced.

Overall, the simulated stresses align well with the measurements. Similar to the z-displacements, the model tends to slightly overpredict stresses during downward bending, pointing to a modeling rather than measurement error. It should be noted that the stresses measured at the strain-gauge location remain well within the elastic regime of the substrate material throughout the process. Consequently, the thermoelastic assumption used to calculate stress from the measured strain signal at the measurement location is fulfilled.

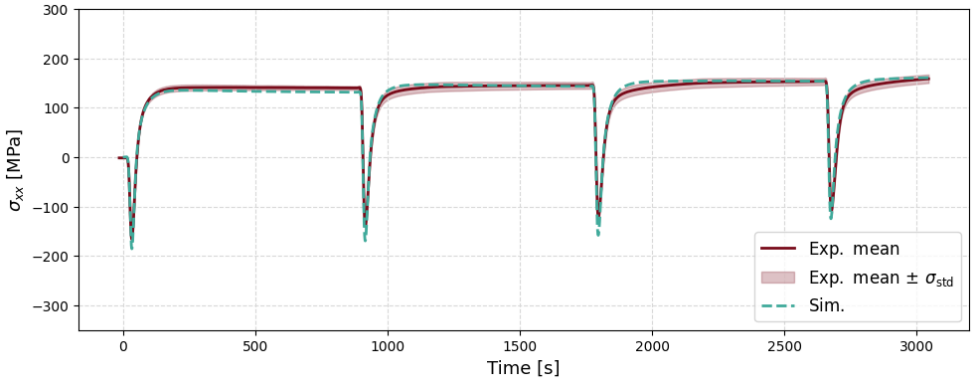

Fig. 12 Stress history – experiment with compensation vs simulation

Finally, Fig. 13 compares the simulated stresses to the experimental stresses without temperature compensation. While the overall trend is captured and the magnitudes are in the expected range, the curve shape deviates significantly. This clearly demonstrates that temperature compensation is essential for obtaining accurate stress history results.

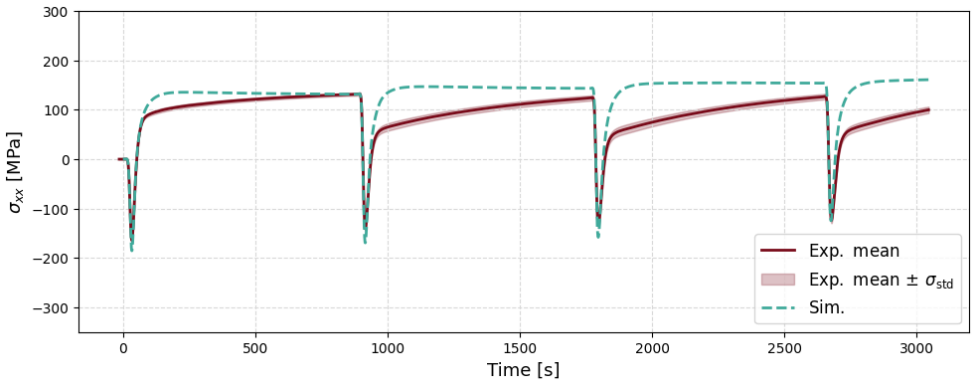

Fig. 13 Stress history – experiment without compensation vs simulation

DISCUSSION

The results of this study demonstrate that high-temperature strain gauges can be successfully applied to capture the transient stress evolution during WA-DED. The scatter between repeated trials was very low, indicating high repeatability of both the experimental setup and the measurement procedure.

Comparison of experimental and numerical results showed only minor deviations in both displacement and strain measurements, underscoring the adequacy of the simulation setup and the applied material model.

For reliable stress measurements, accurate temperature compensation is essential. This requires precise knowledge of the temperature at the gauge location as well as of the substrate's thermal expansion coefficient. Another key limitation is the operational temperature range of the strain gauges. Consequently, stress can only be measured at a certain distance from the weld pool, where an optimum must be found between proximity to the weld and exposure to the maximum mechanical loading.

The installation of strain gauges is laborious, requiring careful surface preparation and controlled curing of the adhesive. In this study, a furnace curing cycle was used to ensure accuracy and reproducibility. However, in many cases such a procedure may not be feasible.

Despite these limitations, the method offers several advantages. Strain gauge measurements are non-destructive, relatively compact compared to optical methods, and capable of delivering time-resolved stress data with high precision. However, pre-existing residual stresses in the substrate can influence the results. For this reason, the strain gauge method is

best suited for analyzing relative changes in stress during the process rather than providing absolute residual stress values.

Overall, the present study demonstrates the feasibility of using high-temperature strain gauges for in-situ monitoring and validation of WA-DED simulations, thereby contributing to more reliable predictive modeling in additive manufacturing."

DECLARATION OF GENERATIVE AI AND AI-ASSISTED TECHNOLOGIES IN THE WRITING PROCESS

During the preparation of this work the authors used ChatGPT to improve the readability and reduce spelling errors. After using this tool, the authors reviewed and edited the content as needed and take full responsibility for the content of the publication.

APPENDICES AND ACKNOWLEDGEMENTS

The consortium would like to thank the federal ministries of Austria for “Climate Action, Environment, Energy, Mobility, Innovation and Technology” (BMK), the ministry of “Labour and Economy” (BMAW), the Austrian Funding Agency (FFG), as well as the four federal funding agencies Amt der Oberösterreichischen Landesregierung; Steirische Wirtschaftsförderungsgesellschaft m.b.H.; Amt der Niederösterreichischen Landesregierung; Wirtschaftsagentur Wien. Ein Fonds der Stadt Wien for funding project “We3D” (FFG Nr. 886184) in the framework of the 8th COMET call.

References

[1] M. FLORIAN, M. OLIVER, P. DOMINIC, U. STEPHAN and S.-B. CHRISTIAN: ‘From CAD model to WAM component: implementation of complex geometries using the example of a hydrogen tank’, *IOP Conf. Ser.: Mater. Sci. Eng.*, Bd. 1315, Nr. 1, S. 012002, Okt. 2024, doi: 10.1088/1757-899X/1315/1/012002.

[2] J. HONNIGE, S. WILLIAMS, M. ROY, P. COLEGROVE and S. GANGULY: *Residual Stress Characterization and Control in the Additive Manufacture of Large Scale Metal Structures*, 2016. doi: 10.21741/9781945291173-77.

[3] F. D. GURMESA, H. G. LEMU, Y. W. ADUGNA and M. D. HARSIBO: ‘Residual Stresses in Wire Arc Additive Manufacturing Products and Their Measurement Techniques: A Systematic Review’, *Applied Mechanics*, Bd. 5, Nr. 3, S. 420-449, Sep. 2024, doi: 10.3390/applmech5030025.

[4] M. BIEGLER, B. GRAF and M. RETHMEIER ‘In-situ distortions in LMD additive manufacturing walls can be measured with digital image correlation and predicted using numerical simulations’, *Additive Manufacturing*, Bd. 20, S. 101-110, März 2018, doi: 10.1016/j.addma.2017.12.007.

[5] X. LU ET AL.: ‘In situ measurements and thermo-mechanical simulation of Ti–6Al–4V laser solid forming processes’, *International Journal of Mechanical Sciences*, Bd. 153-154, S. 119-130, Apr. 2019, doi: 10.1016/j.ijmecsci.2019.01.043.

[6] H. E. COULES, L. D. COZZOLINO, P. A. COLEGROVE and S. W. WEN: ‘Measurement and modelling of the transient thermal-mechanical strain field during GMA welding’, Apr. 2011, accessed: 29. Mai 2024, [Online], available under: https://dspace.lib.cranfield.ac.uk/handle/1826/5820.

[7] K. HOFFMANN: *Eine Einführung in die Messung mit Dehnungsmessstreifen*, Hottinger Baldwin Messtechnik GmbH, Damrstadt, Deutschland, 1987.

[8] ‘Temperaturkompensation bei DMS-Viertelbrücken-Anwendungen’, *HBM*, accessed: 28. August 2025, [Online], available under: https://www.hbm.com/de/10083/temperaturkompensation-bei-dms-viertelbruecken-anwendungen/.

[9] *Werkstoff- und Materialeigenschaften 1.0570*, accessed: 28. August 2025, [Online], available under: https://www.hasco.com/de/werkstoffdatenblatt_1.0570.

[10] C. S. WU, H. G. WANG and Y. M. ZHANG: ‘A New Heat Source Model for Keyhole Plasma Arc Welding in FEM Analysis of the Temperature Profile’, 2006.

[11] P. MICHALERIS: ‘Modeling metal deposition in heat transfer analyses of additive manufacturing processes’, *Finite Elements in Analysis and Design*, Bd. 86, S. 51-60, Sep. 2014, doi: 10.1016/j.finel.2014.04.003.

[12] H. DREXLER, F. HAUNREITER, L. RABERGER, L. REITER, A. HÜTTER and N. ENZINGER: ‘Numerical Modeling of Distortions and Residual Stresses During Wire Arc Additive Manufacturing of an ER 5183 Alloy with Weaving Deposition’, BHM *Berg- und Huettenmaenn. Monatsh.*, Bd. 169, Nr. 1, S. 38-47, Jan. 2024, doi: 10.1007/s00501-023-01421-9.